

Supporting Information

Highly sensitive flux-type non-invasive alcohol biosensor based on direct electron transfer of PQQ-dependent alcohol dehydrogenase adsorbed on carbon nanotubes

Citra Dewi Rakhmania,^a Yoshi Izzudin Azhar,^b Kenji Shida,^c Erika Sinchi,^d Taiki Adachi,^e Keisei Sowa,^e Yuki Kitazumi,^e Osamu Shirai,^e and Masato Tominaga^{*ab}

^aGraduate School of Science and Engineering, Saga University, 1 Honjomachi, Saga 840-8502, Japan.

^bDepartment of Chemistry and Applied Chemistry, Saga University, 1 Honjomachi, Saga 840-8502, Japan.

^cFaculty of Engineering, Kumamoto University, Kumamoto 860-8555, Japan.

^dAnalytical Research Center for Experimental Science, Saga University, 1 Honjomachi, Saga 840-8502, Japan.

^eDivision of Applied Life Sciences, Graduate School of Agriculture, Kyoto University, Sakyo, Kyoto 606-8502, Japan.

*Corresponding author. Email: masato@cc.saga-u.ac.jp

Table of Contents

Experimental Procedures	S- 2
Fig. S1 Pierce™ BCA protein assay kit reaction.	
Fig. S2 Schematic illustration for estimation of enzyme concentration by Pierce™ BCA protein assay kit.	
Fig. S3 UV-VIS spectra of the measurement result of Pierce™ BCA protein assay kit and PQQ-ADH.	
Fig. S4 Calibration curve for Pierce™ BCA protein assay kit.	
Fig. S5 Reaction of ferricyanide reductase activity.	
Fig. S6 Schematic illustration for the experiment of ferricyanide reductase activity.	
Fig. S7 The spectrophotometry results for ferricyanide reductase activity.	
Fig. S8 Schematic illustration for a cascade type of ethanol gas generation.	
Fig. S9 Calibration curve for the cascade type of ethanol gas generation.	
Results and Discussion	S-5
Fig. S10 CVs of PQQ-ADH/MWCNTs/GCE vs. PQQ-ADH/GCE on 0.1 M ethanol detection.	
Fig. S11 Raman spectrum of MWCNTs surface.	
Fig. S12 Electrochemically active surface area (ECSA) of MWCNTs.	
Fig. S13 Schematic of PQQ-ADH surface concentration by QCM measurements.	
Fig. S14 QCM measurements result.	
Fig. S15 QCM result as a function of adsorption time.	
Fig. S16 PQQ-ADH structure.	
Fig. S17 PQQ-ADH size at various molecular orientation.	
Fig. S18 CVs of 0.1 M ethanol detection at CNF film sensor.	
Fig. S19 Investigation methods of stability and reproducibility of reference electrode (PBI/MWCNTs/CNF).	
Fig. S20 Stability and reproducibility test result of R.E (PBI/MWCNTs/CNF) compared to Ag AgCl sat'd KCl.	
Fig. S21 Amperometry response of ethanol gas detection at the CNF film sensor.	
Fig. S22 Various material platforms for the modified film sensor.	
Table S1 Evaluated parameters for various film sensors.	
Fig. S23 Illustration of hydrophobicity degree test method.	
Table S2 Hydrophobicity degree of pure CNF film and MWCNTs modified CNF film.	
Fig. S24 Illustration of ethanol gas diffusion and three-phase interface at CNF film sensor.	
Fig. S25 Photograph of skin gas monitoring system and ethanol skin gas detection for lower dose alcohol consumption.	
Fig. S26 Ethanol skin gas detection at CNF film sensor during higher doses of alcohol consumption.	
Table S3 CNF film sensor vs commercial alcohol sensor efficiency.	
Fig. S27 The effect of heart rate, skin temperature, and body movements on CNF film sensor noises.	
References	S-20

Experimental Procedures

PQQ-ADH Activity Measurement

Enzyme concentration (Pierce™ BCA protein assay kit). This method is used to quantify the total protein. Based on the colorimetric detection of Cu^{2+} reduction to Cu^+ by protein, this measurement occurred in an alkaline medium using a unique reagent containing bicinchoninic acid, as seen in Figure S1. The chelation reaction between 2 molecules of BCA with 1 ion cuprous (in step 2 Figure S1) results in a purple-colored reaction (as in Figure S2).

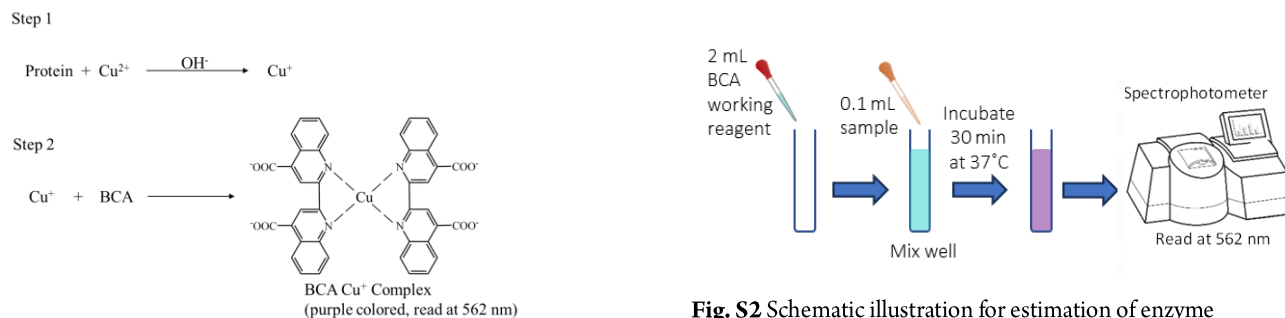


Fig. S1 Pierce™ BCA protein assay kit reaction.

Fig. S2 Schematic illustration for estimation of enzyme concentration by Pierce™ BCA protein assay kit.

This reaction can be observed by UV-VIS at 562 nm, where the absorbance is linear with the increasing protein concentrations. A series of dilutions with known (BSA) protein concentrations are prepared and assayed alongside the test sample. Then, the total protein of the test sample is determined based on the standard curve of BSA protein. The standard procedure for the test tube (sample to working reagent ratio 1:20) is described as follows: At first, the diluted albumin (BSA) standards were prepared by diluting BSA in the same diluent used in the sample with the final BSA concentration ranging from 25-2000 $\mu\text{g}/\text{mL}$. The dilution table guide to prepare protein standards was listed in the manual procedure.¹ 50 parts of the 'A' solution and 1 part of 'B' were mixed (Reagent A: B = 50:1) to form a BCA working reagent. Each 0.1 mL of standard sample was mixed with 2 mL of working reagent and covered. The mixed solution was then incubated at 37°C for 30 minutes. Then, all the tube tests were cooled to room temperature and observed at 562 nm by UV-VIS within 10 minutes. The UV-VIS result is shown in Figure S3. The corrected absorbance for each sample counted as the sample absorbance at 562 nm subtracted by the blank standard (0 $\mu\text{g}/\text{mL}$) absorbance. A standard curve was then prepared by plotting each BSA standard vs. its concentration in $\mu\text{g}/\text{mL}$. This calibration curve was then used to determine the protein concentration of the test sample (Figure S4).

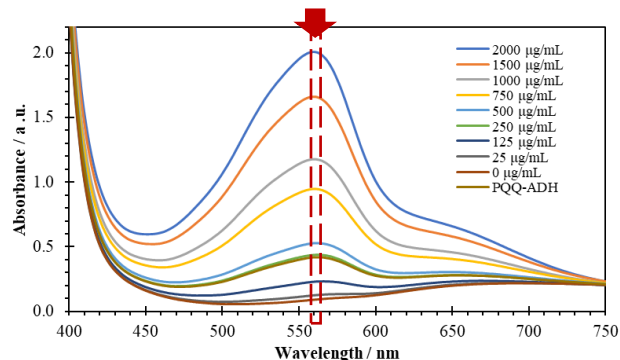


Fig. S3 UV-VIS spectra of the measurement result of Pierce™ BCA protein assay kit and PQQ-ADH.

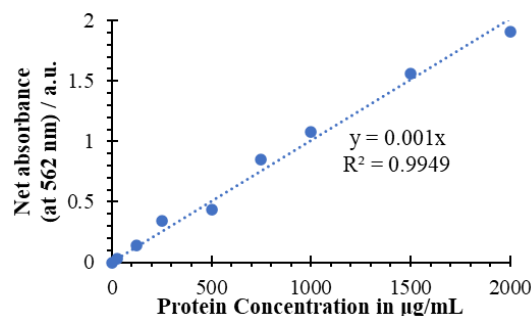


Fig. S4 Calibration curve for Pierce™ BCA protein assay kit.

Ferricyanide reductase activity (spectrophotometry). This method was measured by calorimetrically using potassium ferricyanide as an electron acceptor as illustrated in Figure S5. The ferricyanide reduction reaction occurred when ethanol was added to the solution containing PQQ-ADH, which reduced the greenish color of ferricyanide into a more transparent solution. This reduction reaction can be observed at the absorbance of 417 nm (as shown in Figure S6). Various volumes of PQQ-ADH (2.5, 5, 7.5, 10 μL) were added into 3 mL of 1 mM $\text{Fe}(\text{CN})_6^{3-}$ solution and then mixed thoroughly. Then, 10 mM ethanol was added, mixed, and observed by the spectrophotometer at 417 nm for 60 seconds. The ferricyanide reductase spectrophotometry result is shown in Figure S7. The absorbance result was then calculated by using Equation S1-S5. The result was then calculated as the average enzyme activity. One unit of these activities was defined as the amount of enzyme oxidizing 1 μmol of ethanol per minute.²

$$m_{PQQ-ADH}(g) = PQQ - ADH \text{ concentration } \left(\frac{mg}{mL}\right) \times V_{PQQ-ADH}(mL) \quad (\text{Equation S1})$$

$$Fe \text{ absorbance } (A) = \text{Initial Abs} - \text{Final Abs} \quad (\text{Equation S2})$$

$$Fe \text{ concentration } (c) = A / (\epsilon d) \quad (\text{Equation S3})$$

$$EtOH \text{ concentration } (c) = Fe \text{ concentration } (c) \times \frac{n e^- \text{ of } Fe \text{ red.}}{n e^- \text{ of } EtOH \text{ ox.}} \quad (\text{Equation S4})$$

$$\text{Enzyme Activity } \left(\frac{U}{mg}\right) = \frac{EtOH \text{ concentration } (c)}{m_{PQQ-ADH} (mg) \times \text{time} (min)} \quad (\text{Equation S5})$$

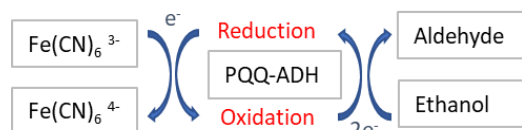


Fig. S5 Reaction of ferricyanide reductase activity.

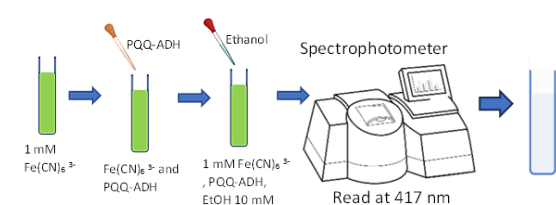


Fig. S6 Schematic illustration for the experiment of ferricyanide reductase activity.

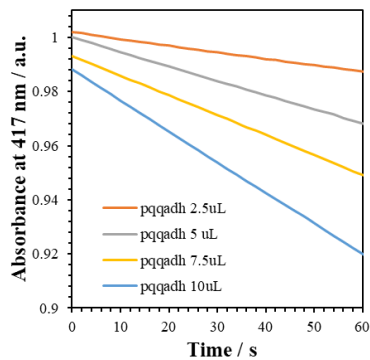


Fig. S7 The spectrophotometry results for ferricyanide reductase activity.

Type of experiment carried out:

1. Solution (using PQQ-ADH/MWCNTs/GCE)
In main text: Figure 2
In ESI: Figure S10, Figure S12, Figure S18
2. Ethanol gas detection by cascade type (Figure S8, using CNF film sensor)
In main text: Figure 4
In ESI: Figure S9, Figure S21
3. Skin gas on the human subject (using CNF film sensor)
In main text: Figure 7
In ESI: Figure S27, Figure S28

Ethanol Gas Detection by Cascade Type (for sensitivity test)

Ethanol gas was evaporated from the cascade-type system, as shown in Figure S8. First, the air was produced in the system using the hand pump. The air was then passed through the water three times before evaporating the ethanol solution. This step was essential to keep the humidity level inside the system to prevent the CNF film sensor from becoming prematurely dehydrated. The continuous air supply subsequently delivered the evaporated ethanol gas to the sensor surface. The CNF film sensor was directly connected to the electrochemical analyzer during the experiment. The current change (by amperometry measurement) was then observed 10 seconds after the air was first introduced to the system. For each concentration observed, the current change was observed for 300 seconds. However, the observed current reached a plateau after 100 seconds, indicating that the ethanol gas produced and circulated in the system was at the same concentration.

The ethanol gas produced by the system was then collected (from 100 seconds to 180 seconds) in a 1 L Tedlar bag for each concentration of the evaporated ethanol solution. The collected gas was analyzed by gas chromatography (GC) to quantify the exact concentration of ethanol gas produced by the cascade-type system in Figure S8. Prior to this experiment, gas chromatography (GC) was calibrated using ethanol gas standard produced by a gas permeator. The concentration of ethanol gas produced in the cascade-type system is shown in Figure S9, where the x-axis shows the concentration of ethanol solution being evaporated in the system, and the y-axis shows the concentration of ethanol gas produced by the system. Thus, the obtained calibration curve (Figure S9) was used to determine the ethanol gas concentration detected during the electrochemical measurements for the CNF film sensor, as in Figure 4(a) and S21.

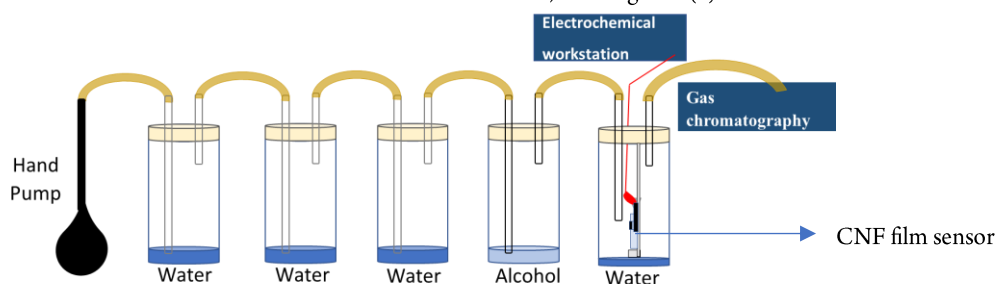


Fig. S8 Schematic illustration for a cascade type of ethanol gas generation.

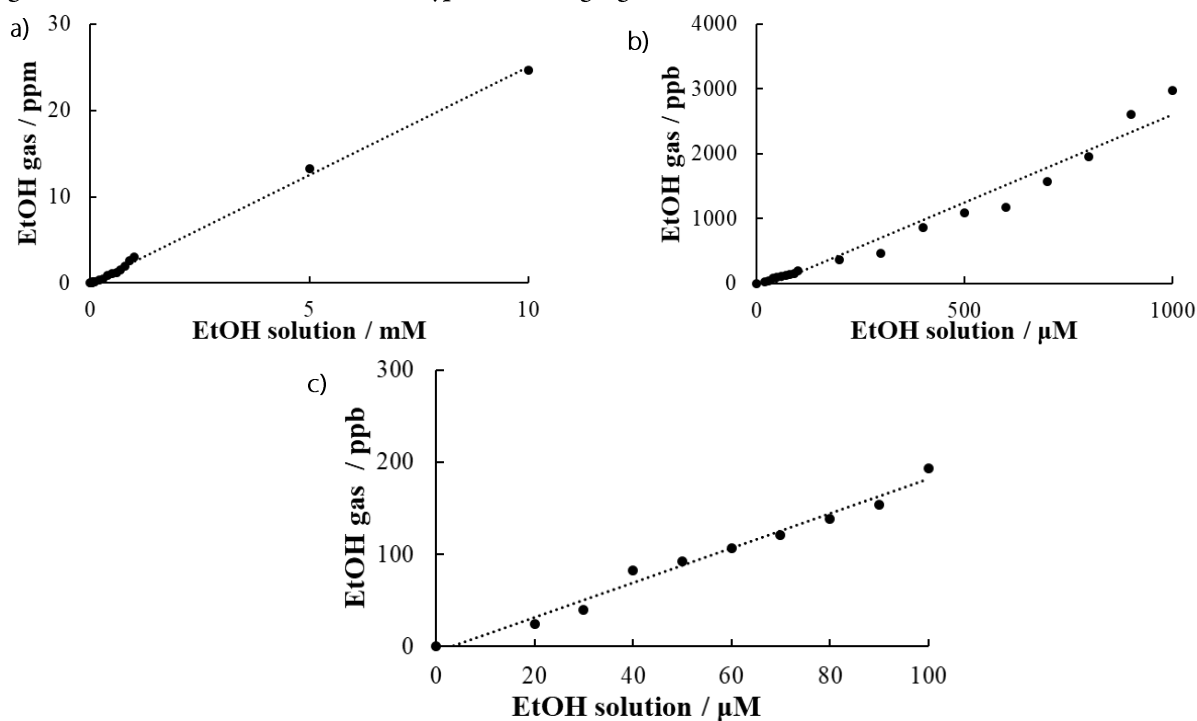


Fig. S9 GC result for the cascade type of ethanol gas generation obtained at (a) 20 μ M up to 10 mM, (b) 20 μ M up to 1 mM (enlarge graph of part a), and (c) 20 μ M up to 100 μ M (enlarge graph of part b) ethanol solutions.

Ethanol Skin Gas Monitoring

For lower-dose alcohol consumption, a subject drank alcohol only once with a dose of 0.04 g/kg body weight within a few seconds. The measurement was then continued until the first skin gas baseline was reached. For higher-dose alcohol consumption, another subject drank alcohol continuously with a dose of 0.5 g/kg body weight with three different concentrations of beverages during the monitoring. The measurement was then continued for an hour.

Results and Discussion

PQQ-ADH/MWCNTs/GCE vs. PQQ-ADH/GCE

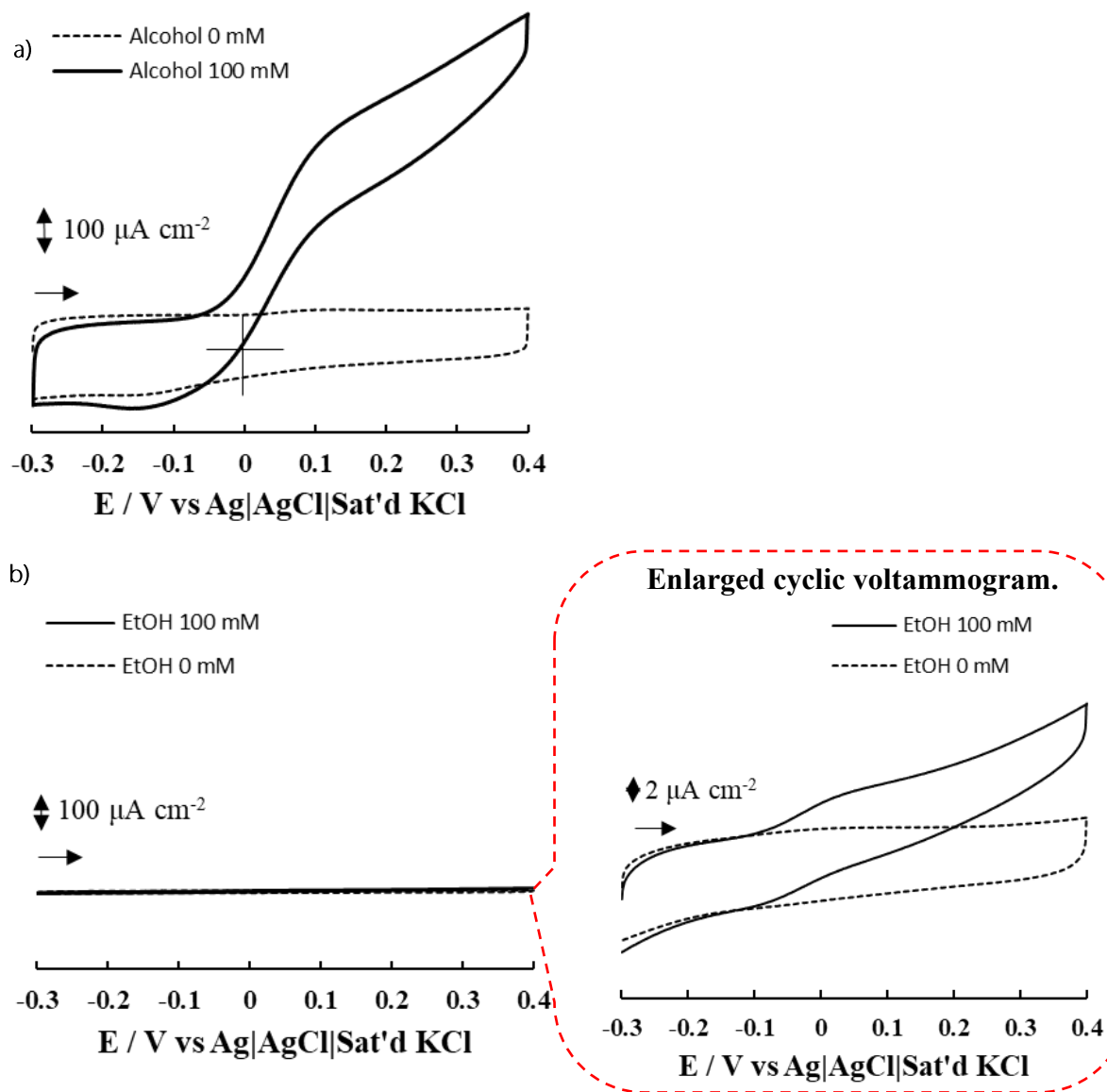


Fig. S10 CVs obtained in 0.1 M acetate buffer solution (pH 5.5) containing CaCl_2 at a scan rate of 10 mV s^{-1} under argon atmosphere at (a) PQQ-ADH/MWCNTs/GCE, and (b) PQQ-ADH/GCE.

Raman Spectra Analysis of MWCNTs

The Raman spectroscopic measurements were performed on a Horiba (Jobin Yvon) LabRAM HR-800 instrument with 514.5 nm (2.41 eV) laser excitation.³ The wavenumber calibration was performed against the 520 cm^{-1} emission of the silica slides used for the analysis. The laser was focused at 2 μm , with the power set at 0.2 mW using a 50x long lens.

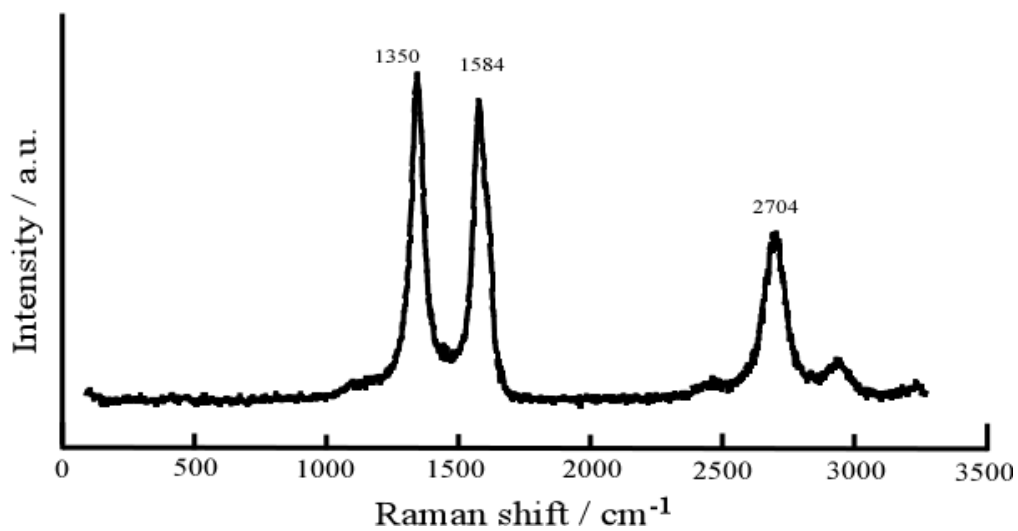


Fig. S11 Raman spectrum of MWCNTs surface.

Electrochemically Active Surface Area (ECSA) of MWCNTs

The ECSA of MWCNTs can be estimated with cyclic voltammetry (CVs) based on rate dependencies. First, the double-layer capacitance (C_{dl}) of MWCNTs on GCE was calculated by plotting the current density difference (ΔJ) in various sweep rates at a fixed potential (-0.3 V vs. Ag|AgCl|saturated KCl). The double-layer capacitance is half of the fitting slope observed in Figure S12B. The ECSA of MWCNTs was then estimated using Equation S6 as in previous report,^{4,18} where the capacitive behavior (C_s) is ca. $2\text{-}5 \mu\text{F cm}^{-2}$ for the well-ordered graphite structure with a small defect.⁴ The ECSA of MWCNTs was estimated to be 9.6 cm^2 within three times CV measurements.

$$ECSA (\text{cm}^{-2}) = C_{dl} / C_s \quad (\text{Equation S6})$$

$$\Delta J = J_A - J_C \quad (\text{Equation S7})$$

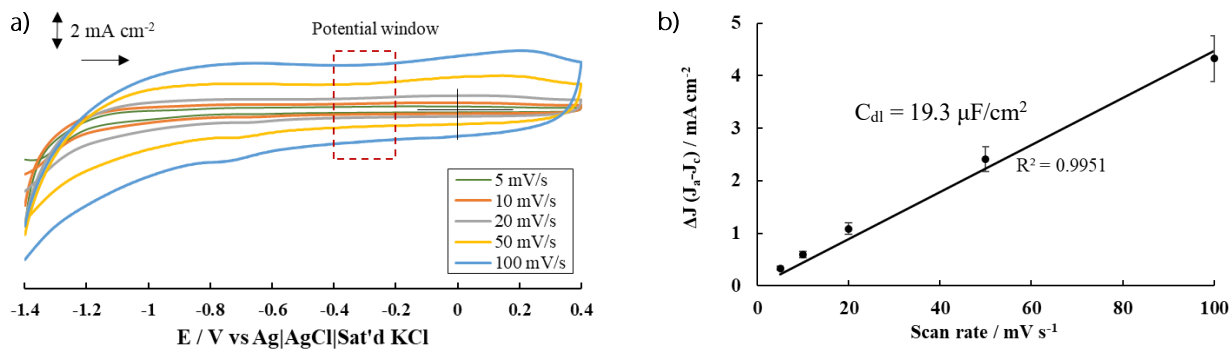


Fig. S12 (a) CV at MWCNTs/GCE in 0.1 M acetate buffer solution (pH 5.5) containing CaCl₂ at various scan rate of (5-100 mV s⁻¹) under argon atmosphere, and (b) linear fitting of scan rates observed vs. current density difference (ΔJ).

PQQ-ADH Surface Concentration by QCM Measurement

QCM method is known as ultra-sensitive towards mass changes.⁵ Therefore, the surface coverage of PQQ-ADH on the MWCNTs/GCE as a function of modification time was measured by QCM based on mass change of the extracted protein of PQQ-ADH adsorbed. At first, GCE-modified MWCNTs were modified with PQQ-ADH enzyme with various adsorption times, as shown in Figure S13. After the desired modification time, the PQQ-ADH modified electrode was gently rinsed with 0.1 M acetate buffer pH 5.5 with 2 mM CaCl₂ to remove excess PQQ-ADH. The modified electrode was then soaked in strong alkaline 100 μ L of 0.3 M NaOH for 1 hour to extract the protein from the modified electrode. The extract solution was then cast and dried onto a surface of polished quartz crystals with a 27 MHz fundamental resonance frequency. The frequency change observed by QCM can be used to calculate mass change by using the Sauerbrey equation (Equation S8). Where Γ is surface concentration, Q is charge obtained by integrating peak area, A is surface area, F is Faraday constant (96,485 C/mol), and n is electron number. A change of 1 Hz is equal to the 30 pg mass change,⁶ hence 1 Hz of frequency changes observed is equal to the mass change per qcm surface area of 0.6 ng/(cm²).^{7,8} The surface concentration of PQQ-ADH can be calculated by Equation S9. The final PQQ-ADH mass change observed by QCM was calculated as per square cm of MWCNT (Figure 3B) instead of as per square cm of QCM (Figure S15). The calculation was conducted using Equation S10. Meanwhile, the number of PQQ-ADH layers formed on MWCNTs surface can be calculated in Equation S11.

$$\text{Sauerbrey Equation: } \Delta F = \frac{2F_0^2}{A \times (\mu_q \rho_q)^{1/2}} \times \Delta m \quad (\text{Equation S8})$$

$$\Gamma_{\text{PQQ-ADH}} (\text{pmol} \cdot \text{cm}^{-2}) = \frac{\Delta m_{\text{PQQ-ADH}} (\text{g} \cdot \text{cm}^{-2})}{MW_{\text{PQQ-ADH}}} \quad (\text{Equation S9})$$

$$\Delta m_{\text{PQQ-ADH}} (\mu\text{g} \cdot \text{cm}^{-2} \text{MWCNTs}) = \frac{\Delta m_{\text{PQQ-ADH}} (\mu\text{g} \cdot \text{cm}^{-2} \text{QCM})}{\text{ECSA}_{\text{MWCNTs}} (\text{cm}^2)} \times A_{\text{QCM}} (\text{cm}^2) \quad (\text{Equation S10})$$

$$\text{Number of PQQADH layer} = \frac{\Gamma_{\text{PQQ-ADH}} (\text{pmol} \cdot \text{cm}^{-2})}{\Gamma_{\text{max. monolayer}} (\text{pmol} \cdot \text{cm}^{-2})} \quad (\text{Equation S11})$$

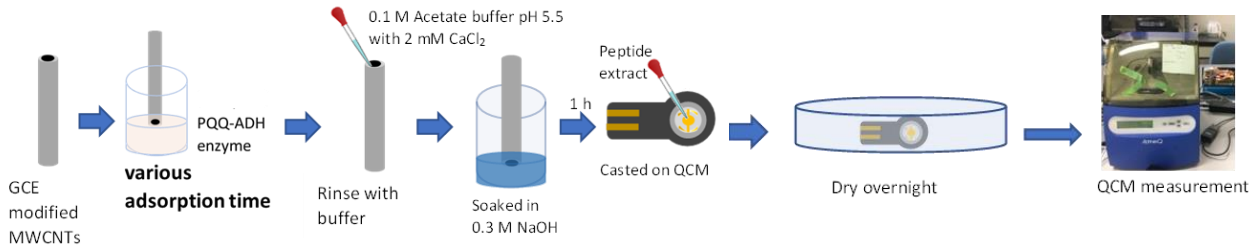


Fig. S13 Evaluation method for PQQ-ADH surface concentration by QCM measurements.

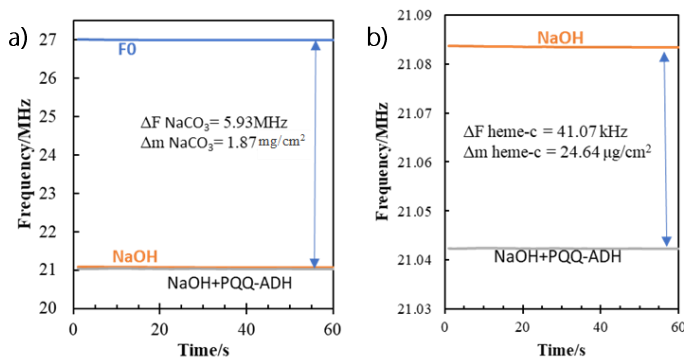


Fig. S14 QCM measurement result of (a) NaOH as a background and (b) PQQ-ADH for 30 minutes adsorption time.

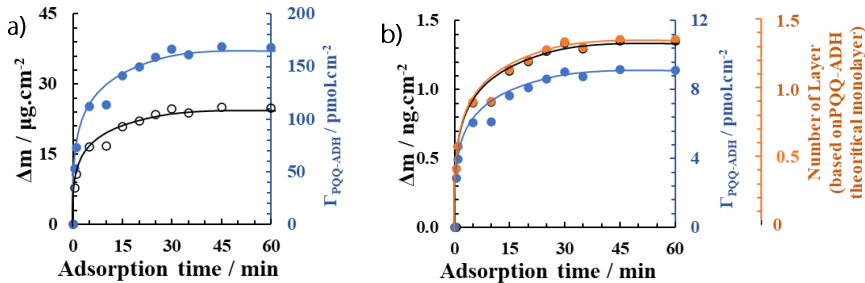


Fig. S15 (a) QCM results as a function of adsorption time; (b) PQQ-ADH surface concentration per cm² of MWCNTs.

PQQ-ADH size, structure, and monolayer (based on the protein data bank of 8GY2)

The size of each PQQ-ADH molecule was estimated to be $70.4 \times 117.4 \text{ \AA}$, hence the diameter of PQQ-ADH ca. $9 \pm 2 \text{ nm}$. The molecular weight of PQQ-ADH for Subunits I, II, and III were 85 kDa, 49 kDa, and 14 kDa, respectively.⁹ Thus, PQQ-ADH's theoretical maximum monolayer level was ca. $2.4\text{--}6.7 \text{ pmol/cm}^2$.

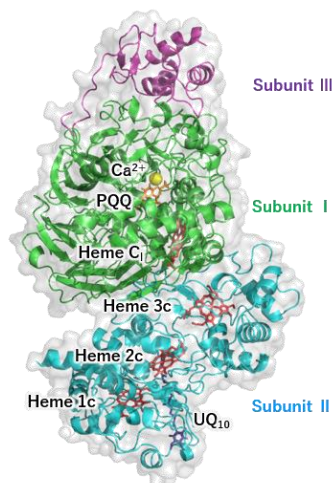


Fig. S16 PQQ-ADH structure.

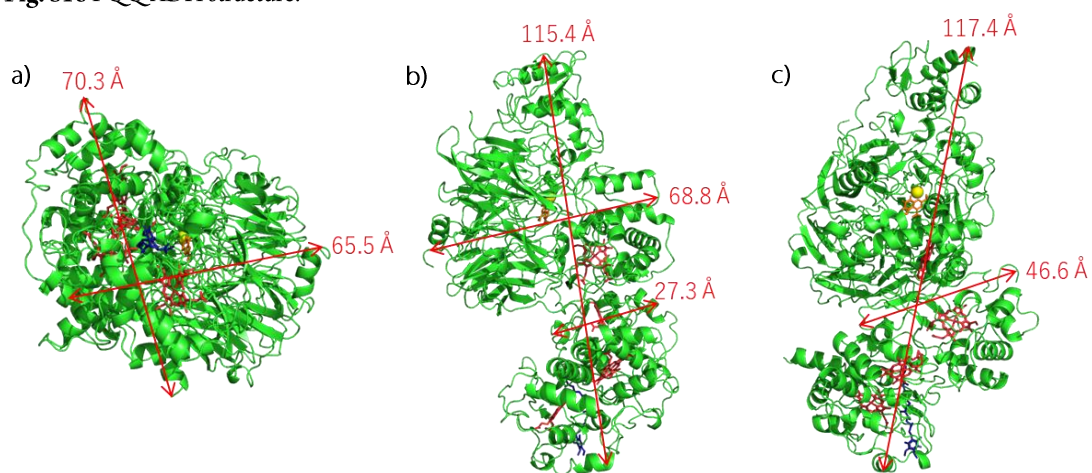


Fig. S17 PQQ-ADH size at various molecular orientations.

Three-Electrode System of CNF Film Sensor

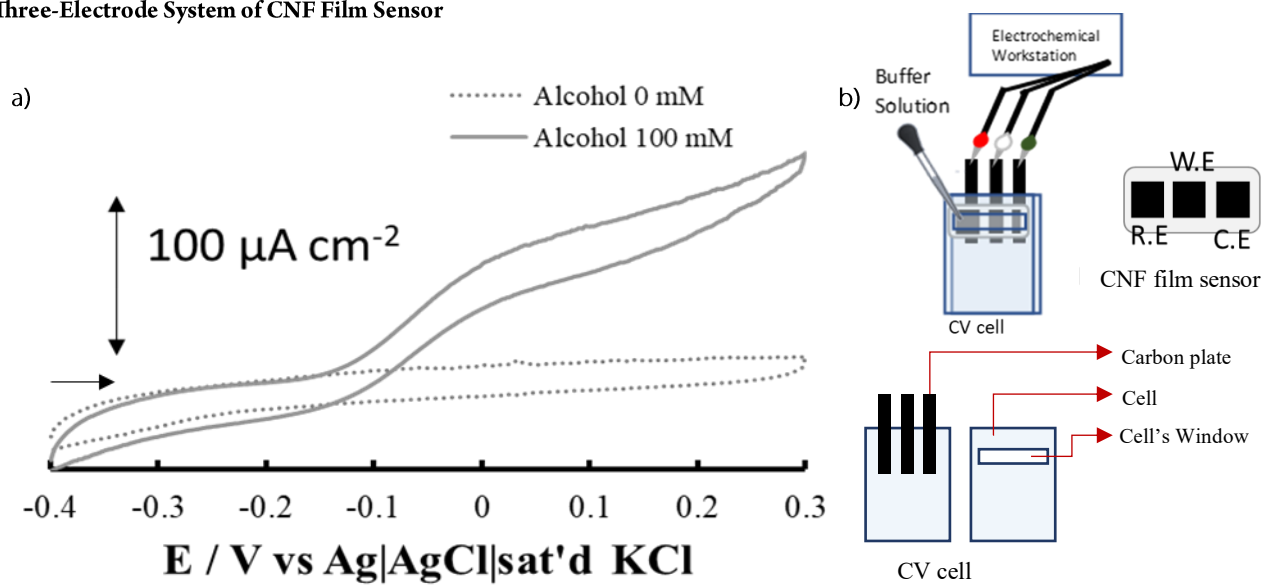


Fig. S18 (a) CVs of 0.1 M ethanol detection at CNF film sensor in 0.1 M acetate buffer solution (pH 5.5) containing CaCl_2 at a scan rate of 10 mV s^{-1} under air; (b) details part of CV cell used for CNF film sensor.

Stability and Reproducibility of the Reference Electrode (PBI/MWCNTs/CNF) vs. Ag|AgCl|sat'd KCl

The experiment was carried out 10 times, as illustrated in Figure S19, with measurement time variations of 0, 10, 15 minutes, 1, 2, 3, 4, 5, and 6 hours. The result is shown in Figure S20, where after 10 minutes of soaking in buffer solution, the voltage range deviation of 10 samples of CNF-based reference electrodes was estimated to be ca. 50 ± 20 mV, and the deviation decreased with increasing time.

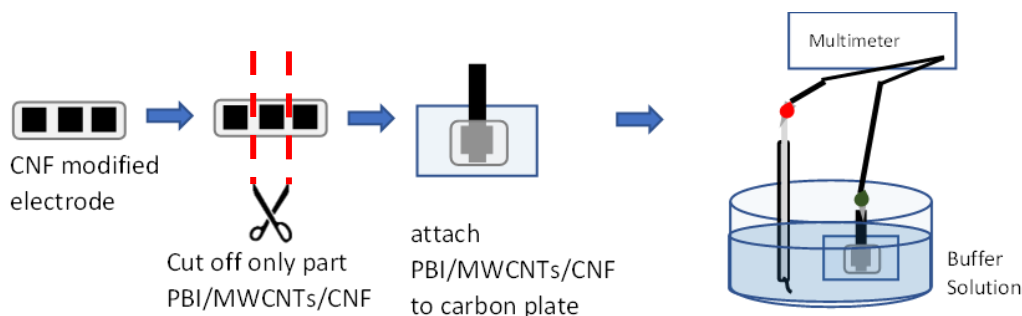


Fig. S19 Experimental method for investigating stability and reproducibility of R.E. vs. Ag|AgCl|sat'd KCl.

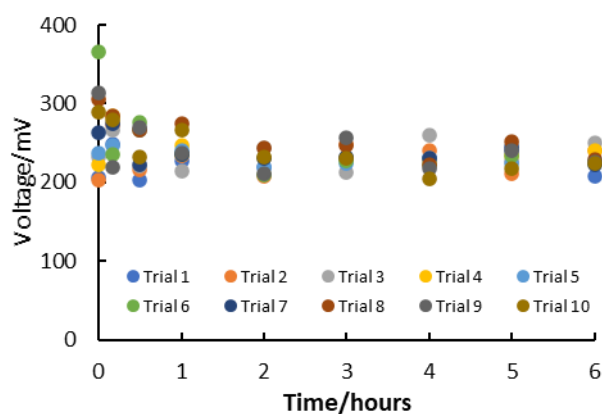


Fig. S20 Plots for stability and reproducibility result of R.E compared to standard reference electrode Ag|AgCl|sat'd KCl.

According to the previous study,^{16,19} the elution of AgCl from Ag|AgCl ink-printed as a reference electrode might greatly reduce the enzyme activity and degrade the biosensor performance. Thus, we decided to use PBI/MWCNTs as reference electrodes. Moreover, the reference electrode prepared using the PBI/MWCNTs exhibited high stability and repeatability in a laboratory environment (Figure S20).

However, we suspect that the drift in the reference electrode potential of our CNF electrodes in on-skin measurements caused the resulting signal to drift, so we discarded 3/8 on-skin data sets for this reason.

Sensitivity of CNF Film Sensor for Alcohol Gas Detection

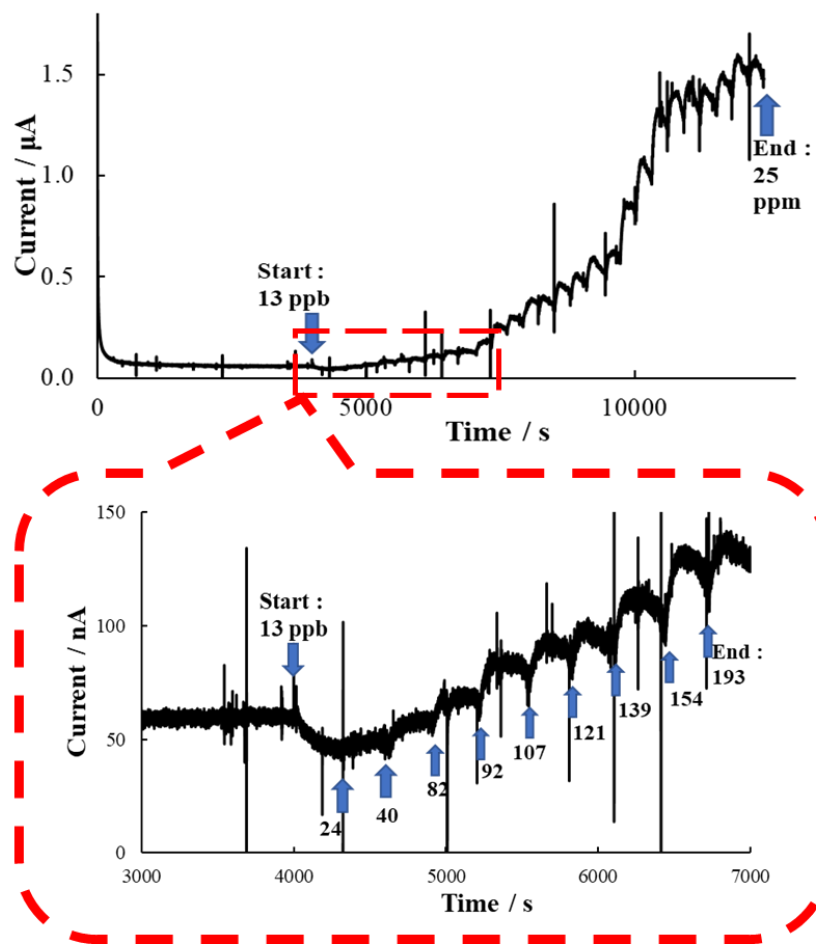


Fig. S21 Amperometry response of ethanol gas detection at the CNF film sensor. Potential detection at 0.2 V vs. Ag|AgCl|saturated KCl.

The actual potential for amperometry measurement was 0 V vs. the PBI/MWCNT's reference electrode. We tried amperometry measurement for a higher potential at 0.1 V vs. the PBI/MWCNT's reference electrode, but the results showed higher deviations in lower concentrations (ppb level).

CNF vs. Other Material as a Modified Platform Sensor

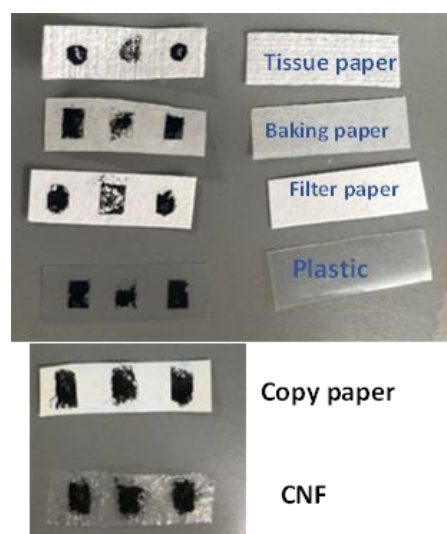


Fig. S22 Various material platforms for the modified film sensor.

Table S1 Evaluated parameters for various film sensors.

Platform	Thick. / μm	weight / mg	Water abs. / mg	Evap. rate / $\text{mg} \cdot \text{min}^{-1} \cdot \text{cm}^{-2}$	Hydrophobicity		Catalytic Oxidation Current density ^(*) at $0.1\text{V} / \mu\text{A cm}^{-2}$	Detection range ^(*) / ppb
					Unmodified	After MWCNTs modified		
Tissue paper X70	15	11.9	90.5	0.51	No	No	-	-
Filter paper 40 ϕ	27	15.2	35.5	0.49	No	No	-	-
Baking paper	56	5.1	5.3	0.09	Yes	Yes	28.9	2900-366000
Plastic	57	7	-	-	Yes	Yes	73.55	2900-366000
Copy paper	95	8.0	21.9	0.47	Yes (≤ 5 mins)	Yes (≤ 5 mins)	32.92	361-345000
CNF	10	0.7	19.7	0.63	No	Yes	125.83	24-25000

^(*) Measurement methods are illustrated in Figure S18.

^(*) Observed by air-cascade type as in Figure S8.

Hydrophobicity Degree Test

The experiment was carried out as illustrated in Figure S23 for both pure CNF film and MWCNTs modified CNF. First, 10 μ L water was dropped on the platform, tested, and observed. The water interface degree on the platform was analyzed and categorized as follows:

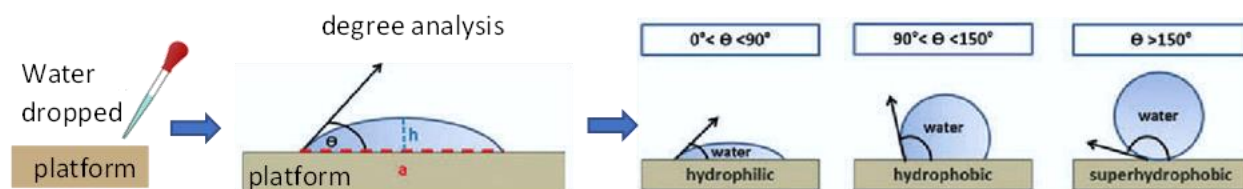



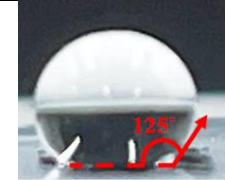

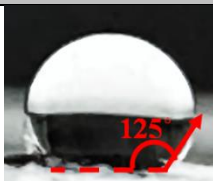
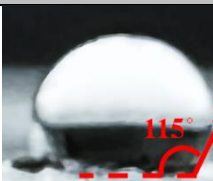


Fig. S23 Illustration of hydrophobicity degree test method.

Table S2 Hydrophobicity degree of pure CNF film and MWCNTs modified CNF film.

Platform	Unmodified	Modified with MWCNTs		
		5s	1 min	5 min
CNF	 Hydrophilic (0°)	 Hydrophobic (135°)	 Hydrophobic (135°)	 Hydrophobic (125°)
		Modified with MWCNTs		
		10 min	20 min	30 min
CNF		 Hydrophobic (125°)	 Hydrophobic (125°)	 Hydrophobic (115°)

Ethanol Gas Diffusion at CNF film sensor

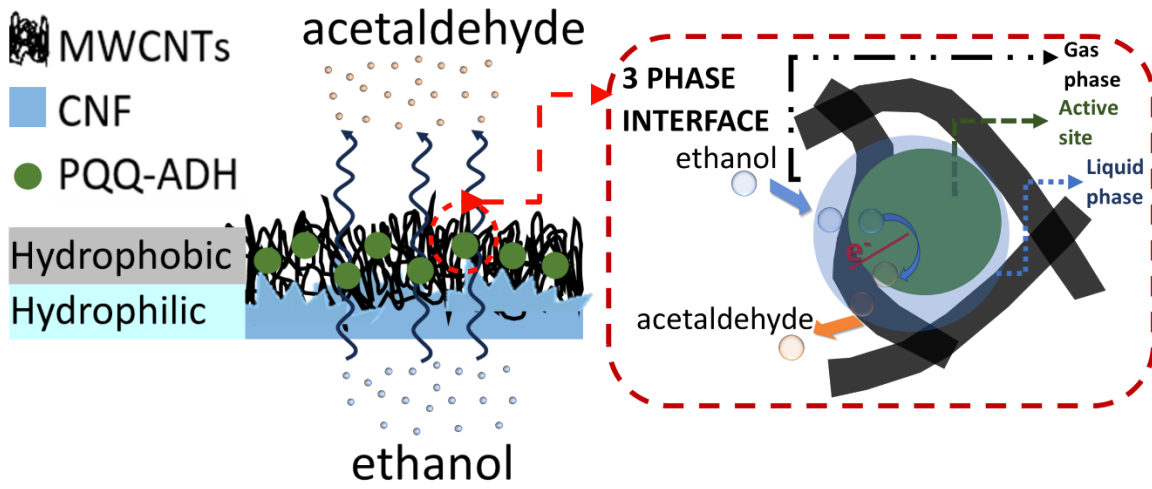


Fig. S24 Illustration of ethanol gas diffusion and three-phase interface at the cellulose nanofiber (CNF) film sensor.

Ethanol Gas Monitoring on the Human Subject

Before this experiment was carried out, the alcohol consumption dose should be decided, and the mass of ethanol consumption needed to be calculated by using:

$$\text{mass of ethanol consumed (gram)} = \text{dose} \left(\frac{\text{g ethanol}}{\text{kg body weight}} \right) \times \text{subject body weight (kg)} \quad (\text{Equation S12})$$

Then, the volume of alcohol needed for a certain alcohol percentage can be calculated based on the reference [13]:

$$\text{mass of ethanol (g)} = \% \text{Alcohol in volume} \times \rho_{\text{ethanol}} \times \text{volume of typical alcohol drink (mL)} \quad (\text{Equation S13})$$

% alcohol in volume is the percentage of alcohol content in a typical alcoholic drink, usually found on the alcohol drink label. ρ_{ethanol} is 0.79.

Lower dose alcohol consumption

The alcohol gas amperometry baseline was measured for ca. 16 min before drinking the alcohol. At this time, a subject (with conditions overnight fasting 10 h) drank alcohol only one time during the experiment with a dose of 0.04 g/kg body weight within a few seconds. This dose is equal to 2.64 g ethanol or 22.34 mL of Alcohol 15%. The measurement was then continued until the first skin gas baseline was reached.

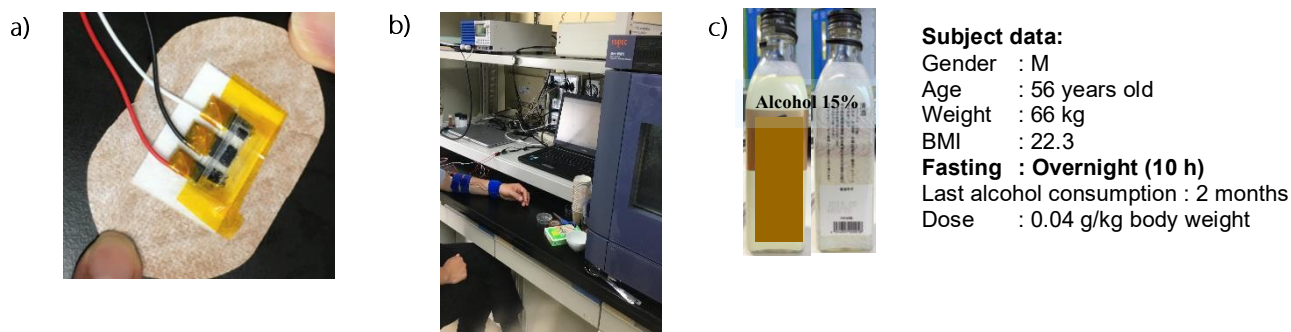


Fig. S25 Photograph of (a) skin gas monitoring system, (b) ethanol gas detection for lower dose alcohol consumption, and (c) type of alcoholic beverages drank by subject.

Higher dose alcohol consumption

This time, another subject drank alcohol continuously with a dose of 0.5 g/kg body weight with three different concentrations of beverages during the monitoring. The alcohol gas baseline was first measured for 16 min before started to drink alcohol. In total, the subject drank 46.5 g of ethanol, which is 350 mL of Alcohol 5% (Beer), 130 mL of Alcohol 12%, and 60 mL of Alcohol 43%. During the monitoring, the subject was under non-fasting conditions where he ate snacks while drinking alcohol. The measurement was then continued for an hour.

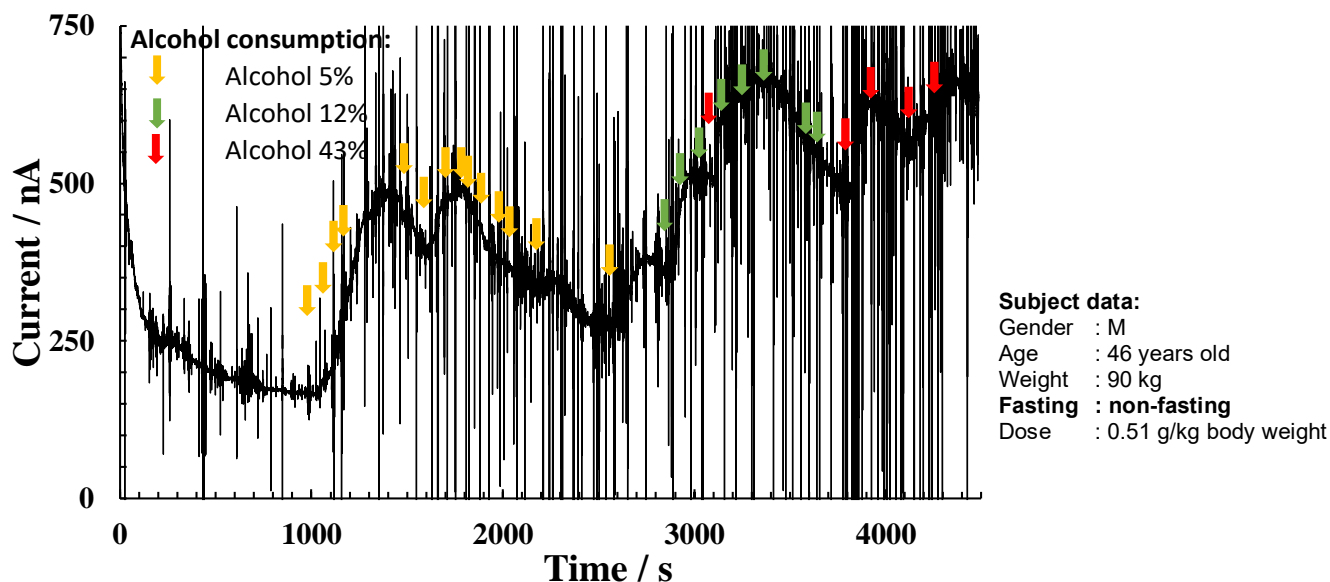


Fig. S26 Ethanol gas detection at CNF film sensor during higher dose of alcohol consumption under non-fasting conditions.

Based on data from Figure S27,

Alcohol 5%: 1 can beer = 350 mL

mass of ethanol = $5\% \times 0.79 \times 350 = 13.8$ g

1 sip of drink = $350/14 = 25$ mL ≈ 0.9875 g

Alcohol 12%: ca. 130 mL

mass of ethanol = $12\% \times 0.79 \times 130 = 12.3$ g

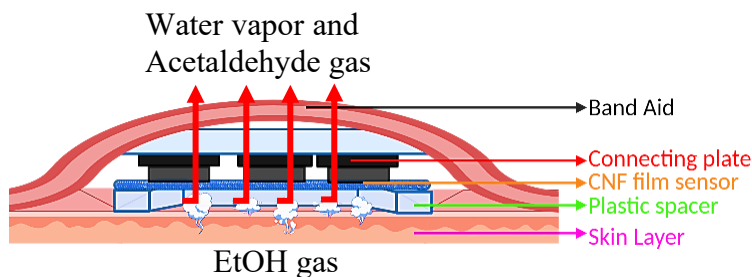
1 sip of drink = $130/8 = 16.8$ mL ≈ 1.6 g

Alcohol 43%: ca. 60 mL

mass of ethanol = $43\% \times 0.79 \times 60 = 20.4$ g

1 sip of drink = $60/5 = 12$ mL ≈ 4.08 g

Illustration of water evaporation at CNF film sensor:



We have successfully monitored ethanol gas on human skin for 8 experiments, with a success rate of 62.5%. The remaining 37.5% failure rate was possibly due to the instability of the reference electrode.

The increased leakage current observed on the skin ca. 150 ± 50 nA, measured in the absence of consumed alcohol (baseline at Figure 7 and S26), possibly caused by the increased temperature on the skin (36.7 °C) as compared to our laboratory measurements or potential instability of the reference electrode. The leakage current observed in the laboratory at 25 ± 3 °C was approximately ca. 50 ± 20 nA (Figure S21). Baseline (leakage) current stability still remains a challenge for the CNF film sensors.

CNF film sensor flux and sensor efficiency

Based on [15] sensor flux, sensor activity, skin permeability and sensor efficiency can be calculated by :

$$Flux \left(\frac{mol}{cm^2 s} \right) = \frac{i (A)}{n \times F \left(\frac{sA}{mol} \right) \times Skin \text{ area observed } (cm^2)} \quad (\text{Equation S14})$$

$$\alpha_{sensor} \left(\frac{cm}{s} \right) = \frac{i (A)}{C \times n \times F \left(\frac{sA}{mol} \right) \times Skin \text{ area observed } (cm^2)} \quad (\text{Equation S15})$$

$$k_{skin} \left(\frac{cm}{s} \right) = \frac{Flux \left(\frac{mol}{cm^2 s} \right) \times Ethanol \text{ molecular weight} \times 1000 \left(\frac{cm^3}{L} \right)}{BAC \left(\frac{g}{L} \right)} \quad (\text{Equation S16})$$

$$k_{skin} \left(\frac{cm}{s} \right) = \frac{D \left(\frac{cm^2}{s} \right)}{L (cm)} \quad (\text{Equation S17})$$

$$\bar{\alpha} = \frac{\alpha_{sensor} \left(\frac{cm}{s} \right)}{k_{skin} \left(\frac{cm}{s} \right)} \quad (\text{Equation S18})$$

Where sensor flux can be calculated by equation S14, i is current (A), n is the number of electrons, F is Faraday constant 9.64×10^4 (s A/mol), α is sensor activity (cm/s), k_{skin} is skin permeability (cm/s), BAC is blood alcohol concentration (g/L), D is diffusion coefficient of ethanol in the skin (cm²/s), L is the rate-limiting layer of skin thickness (cm), $\bar{\alpha}$ is relative sensor rate constant in relation to skin permeability.

Theoretical BAC was calculated according to [13,14]:

$$mass \text{ of ethanol consumed } (g) = body \text{ weight } (kg) \times Volume \text{ of distribution } \left(\frac{L}{kg} \right) \times \left[BAC_t \left(\frac{g}{L} \right) + [zero - order \text{ elimination rate } \left(\frac{g}{Lh} \right) \times time \text{ from strated to drink } (h)] \right] \quad (\text{Equation S19})$$

Where,

The volume of distribution (V_d) refers to a theoretical volume of fluid in which a drug is distributed to blood and can be calculated as:

$$V_d = \frac{[total \text{ water in body } (L) / bodyweight (kg)]}{water \text{ in blood } \left(\frac{g}{100 mL} \right)} \quad (\text{Equation S20})$$

While,

Total water in the body (TBW) can be calculated using:

$$TBW \text{ in men } (L) = 2.447 - [0.09516 \times age (year)] + [0.1074 \times height (cm)] + [0.3362 \times weight (kg)] \quad (\text{Equation S21})$$

$$TBW \text{ in women } (L) = -2.097 + [0.1069 \times height (cm)] + [0.2466 \times weight (kg)] \quad (\text{Equation S22})$$

Table S3 CNF film sensor vs commercial alcohol sensor efficiency

Sensor	Rate limiting layer	$k_{skin} / \times 10^6 \text{ cm s}^{-1}$	$\alpha_{sensor} / \times 10^7 \text{ cm s}^{-1}$	$\bar{\alpha}$	Sensor type	Ref.
ION RAP	Stratum corneum	0.3	1.3	0.4	Robin	[15]
WrisTAS	Stratum corneum	0.53	2.45	0.75	Robin	[15]
ION wearable	Stratum corneum	0.33	100	31	Flux	[15]
CNF film sensor	Skin layer (Epidermis + Dermis)	2.7±0.5	8000	363	Flux	Our work

The CNF film sensor showed a higher sensor rate constant ($\bar{\alpha}$) than the previously reported sensor due to higher sensor activity (α_{sensor}). The result also showed that the subject's skin permeability was nine times higher than the previously reported value. These two factors are essential to achieving fast response in the sensor.

The effect of heart rate, skin temperature and mechanical movement to sensor noises

This experiment was carried out by attaching the CNF film sensor on human skin without alcohol consumption. Then the effect of each parameter was observed.

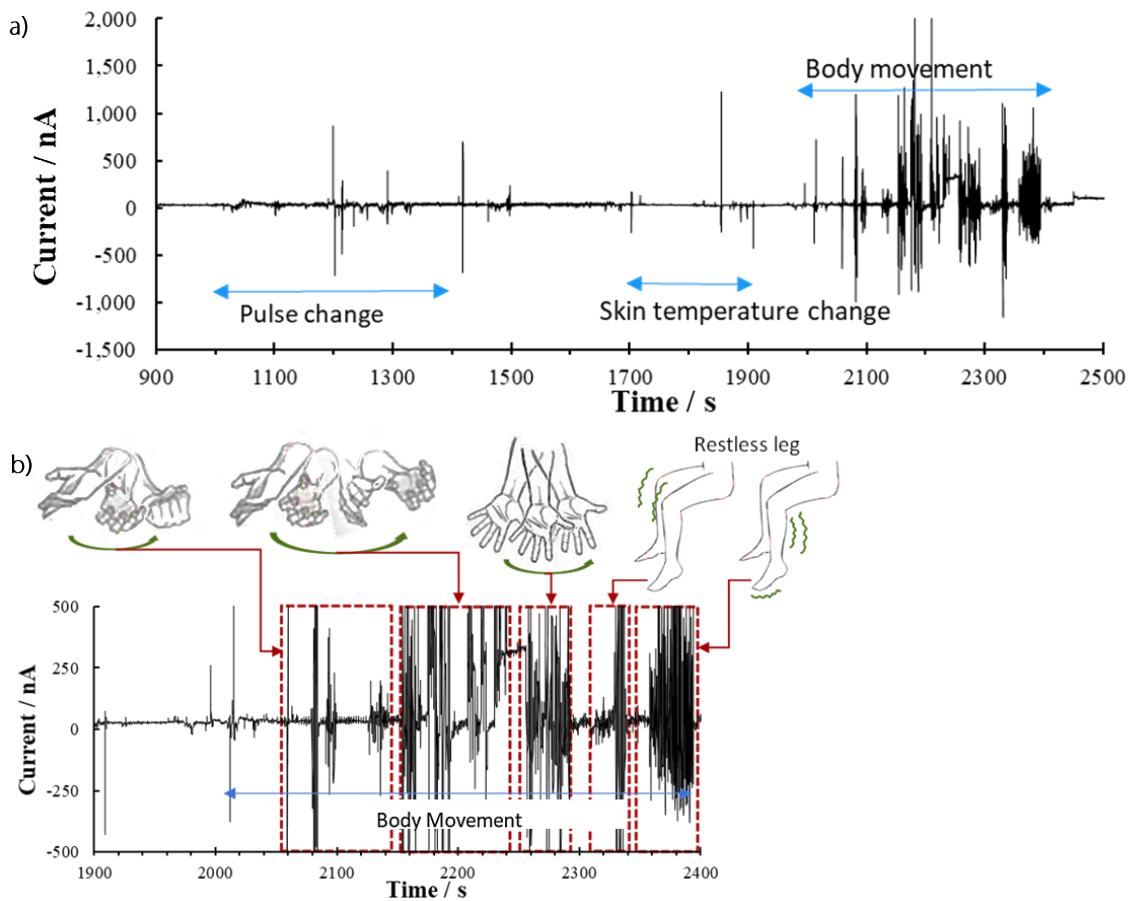


Fig. S27(a) The effect of heart rate, skin temperature and body movements to CNF film sensor noises; and (b) enlarge part of the effect body movements.

References

- (1) ThermoScientific, "Pierce™ BCA Protein Assay Kit", can be found under https://assets.thermofisher.com/TFS-Assets/LSG/manuals/MAN0011430_Pierce_BCA_Protein_Asy_UG.pdf, 2020 (accessed 17/01/2024).
- (2) Matsushita, K.; Yakushi, T.; Toyama, H.; Shinagawa, E.; Adachi, O. Function of multiple heme c moieties in intramolecular electron transport and ubiquinone reduction in the quinoxinoprotein alcohol dehydrogenase-cytochrome c complex of *Gluconobacter suboxydans*. *J. Biol. Chem.* **1996**, 271, 4850-7.
- (3) Tominaga, M.; Iwaoka, A.; Kawai, D.; Sakamoto, S. Correlation between carbon oxygenated species of SWCNTs and the electrochemical oxidation reaction of NADH. *Electrochem. Comm.* **2013**, 31, 76–79.
- (4) Sari, S. R.; Tsushida, M.; Sato, T.; Tominaga, M. Highly sensitive detection of phosphate using well-ordered crystalline cobalt oxide nanoparticles supported by multi-walled carbon nanotubes. *Mater. Adv.* **2022**, 3, 2018–2025.
- (5) Sauerbrey, G. Verwendung von Schwingquarzen zur Wägung dünner Schichten und zur Mikrowägung. *Zeitschrift für Physik.* **1959**, 155(2), 206–222.
- (6) Tominaga, M.; Tamai, S.; Nakao, S.; Miyamoto, M.; Satomura, T. High electrochemical stability of hyperthermophilic archaeal multicopper enzyme adsorbed on gold electrodes compared to fungal laccase. *Electrochem. Comm.* **2022**, 136, 107222.
- (7) Tominaga, M.; Ohtani, M.; Taniguchi, I. Gold single-crystal electrode surface modified with self-assembled monolayers for electron tunneling with bilirubin oxidase. *PCCP* **2008**, 10(46), 6928.
- (8) Tominaga, M.; Ohira, A.; Yamaguchi, Y.; Kunitake, M. Electrochemical, AFM and QCM studies on ferritin immobilized onto a self-assembled monolayer-modified gold electrode. *J. Electroanal. Chem.* **2004**, 566(2), 323–329.
- (9) Adachi, T.; Miyata, T.; Makino, F.; Tanaka, H.; Namba, K.; Kano, K.; Sowa, K.; Kitazumi, Y.; Shirai, O. Experimental and Theoretical Insights into Bienzymatic Cascade for Mediatorless Bioelectrochemical Ethanol Oxidation with Alcohol and Aldehyde Dehydrogenases. *ACS Catal.* **2023**, 13, 7955–7965.
- (10) Latour, R. A. The Langmuir isotherm: A commonly applied but misleading approach for the analysis of protein adsorption behavior. *J. Biomed. Mater. Res. A*, **2014**, 103(3), 949–958.
- (11) Bayuo, J.; Pelig-Ba, K. B.; Abukari, M. A. Isotherm modeling of lead (II) adsorption from aqueous solution using groundnut shell as a low-cost adsorbent. *IOSR-JAC.* **2018**, 11(1), 18–23.
- (12) Lee, J.M. *Chapter 2: Enzyme Kinetics in Biochemical Engineering*. Prentice-Hall Inc.: Pullman, **1992**, pp 2-1 - 2-46.
- (13) Jones, A.W. Alcohol, its absorption, distribution, metabolism, and excretion in the body and pharmacokinetic calculations. *WIREs Forensic Sci.*, **2019**, 1, e1340.
- (14) Gullberg, R. G.; Jones, A. W. Guidelines for estimating the amount of alcohol consumed from a single measurement of blood alcohol concentration: re-evaluation of Widmark's equation. *Forensic science international*, **1994**, 69(2), 119–130.
- (15) Lansdorp, B. M. Flux-Type versus Concentration-Type Sensors in Transdermal Measurements. *Biosensors*, **2023**, 13(9), 845.
- (16) Makizuka, T.; Sowa, K.; Shirai, O.; Kitazumi Y. Inhibition of direct-electron-transfer-type bioelectrocatalysis of bilirubin oxidase by silver ions. *ANAL. SCI.*, **2022**, 38, 907–912.
- (17) Lansdorp, B. M.; Lamberg, P.; Hamid, R. Screen-Printed Silver/Silver Chloride Electrodes Inhibit Alcohol Oxidase Activity. *ECS sensors plus*, **2023**, 2(3), 030602.
- (18) Zhou, C.-A.; Wang, S.; Ma, K.; Song, L.; Zheng, L.; Yue, H. Membrane-free pure H₂ production over single dispersed Ru-anchored Pt₃Ni alloys via coupling ethanol selective electrooxidation. *Appl. Catal., B.*, **2023**, 321, 122065.